Journal of Hydrology 364 (2009) 227–235

Contents lists available at ScienceDirect

Journal of Hydrology

journal homepage: www.elsevier.com/locate/jhydrol

# Satellite-based prediction of rainfall interception by tropical forest stands of a human-dominated landscape in Central Sulawesi, Indonesia

Jens Nieschulze [a,*,1], Stefan Erasmi [b], Johannes Dietz [c,d,2], Dirk Hölscher [c]

[a] Institute of Forest Biometrics and Informatics, University of Göttingen, Büsgenweg 1, 37077 Göttingen, Germany
[b] Cartography, GIS and Remote Sensing Department, Institute of Geography, University of Göttingen, Goldschmidtstr. 5, 37077 Göttingen, Germany
[c] Tropical Silviculture, Institute of Silviculture, University of Göttingen, Büsgenweg 1, 37077 Göttingen, Germany
[d] Plant Ecology, Albrecht-von-Haller-Institute for Plant Sciences, University of Göttingen, Untere Karspüle 2, 37073 Göttingen, Germany

ARTICLE INFO

*Article history:*
Received 29 October 2007
Received in revised form 2 October 2008
Accepted 31 October 2008

*Keywords:*
Quickbird
Local maxima
Logging
Canopy
Texture

SUMMARY

Rainforest conversion to other land use types drastically alters the hydrological cycle in which changes in rainfall interception contribute significantly to the observed differences. However, little is known about the effects of more gradual changes in forest structure and at regional scales. We studied land use types ranging from natural forest over selectively-logged forest to cacao agroforest in a lower montane region in Central Sulawesi, Indonesia, and tested the suitability of high-resolution optical satellite imagery for modeling observed interception patterns.

Investigated characteristics indicating canopy structure were mean and standard deviation of reflectance values, local maxima, and self-similarity measures based on the grey level co-occurrence matrix and geostatistical variogram analysis. Previously studied and published rainfall interception data comprised twelve plots and median values per land use type ranged from 30% in natural forest to 18% in cacao agroforests. A linear regression model with local maxima, mean contrast and normalized digital vegetation index (NDVI) as regressors was able to explain more than 84% ($R^2_{adj}$) of the variation encountered in the data. Other investigated characteristics did not prove significant in the regression analysis. The model yielded stable results with respect to cross-validation and also produced realistic values and spatial patterns when applied at the landscape level (783.6 ha). High values of interception were rare and localized in natural forest stands distant to villages, whereas low interception characterized the intensively used sites close to settlements. We conclude that forest use intensity significantly reduced rainfall interception and satellite image analysis can successfully be applied for its regional prediction, and most forest in the study region has already been subject to human-induced structural changes.

© 2008 Elsevier B.V. All rights reserved.

## Introduction

Rainfall interception is an important component of the ecosystem water budget especially in tropical montane forests under natural conditions. E.g. in catchments covered by natural rain forest in the Ecuadorian Andes, the rainfall interception amounted to 40% of gross precipitation (Fleischbein et al., 2006). The conversion of natural forest to other land use types may drastically alter the hydrological cycle in which changes in rainfall interception contribute significantly to the observed difference (e.g., Bruijnzeel, 1990; Grip et al., 2005). Changes in land cover type such as forest conversion have been followed up by remote sensing in a series of studies (e.g., FAO, 2001; Achard et al., 2002; Erasmi et al., 2004) and the obtained data may be used for estimations of changes in the carbon budget or hydrological fluxes at a regional scale (Held and Rodriguez, 2005). On the other hand, gradual changes in land cover (land cover modification) as caused by selective forest use are more difficult to include in regional analyses, nonetheless they may be important with respect to their spatial extension and their influences on hydrological fluxes. For different states of the Brazilian Amazon gradual forest disturbances and changes in forest structure caused by selective logging could be identified by satellite data and doubled previous estimates of the total annual extent of forest degraded by human activities (Asner et al., 2005). The effects of forest management on water flows may also be severe and have been reviewed by Chappell et al. (2005). However, with respect to rainfall interception the existing results are somewhat contradictory.

In a lowland forest on Borneo, Central Kalimantan, Indonesia, the rainfall interception was 11% of gross precipitation (Pg) in an

* Corresponding author. Tel.: +49 3641 576138; fax: +49 3641 5770.
*E-mail address:* jniesch@gwdg.de (J. Nieschulze).
[1] Present address: Max-Planck-Institute for Biogeochemistry, P.O. Box 10 01 64, 07701 Jena, Germany.
[2] Present address: Worldagroforestry Centre, P.O. Box 30677-00100 Nairobi, Kenya.

0022-1694/$ - see front matter © 2008 Elsevier B.V. All rights reserved.
doi:10.1016/j.jhydrol.2008.10.024

unlogged natural forest and 6% of Pg in a logged forest (Asdak et al., 1998) which thus points to a decrease in interception with disturbance. In another lowland forest in northern Borneo, Sabah, Malaysia, it was found interception was estimated with 8% of Pg in undisturbed forest and with 15% and 19% of Pg in logged forests, indicating interception rates to increase with disturbance intensity (Chappell et al., 2001). The two studies have in common that they discuss the role of big trees and a changed canopy roughness which may have caused the observed patterns. While Asdak et al. (1998) assumed that the reduced roughness of logged forests reduced the interception, Chappell et al. (2001) suggested that tall trees would also enhance the capture of falling rain drops from turbulent eddies and thus lead to a higher precipitation. In the montane forest zone of Central Sulawesi, however, it was observed that local forest use reduced mean tree heights and that rainfall interception strongly decreased with decreasing mean tree height (Dietz et al., 2006). Together, leaf area index estimated from hemispheric photographs and mean tree height explained 81% of the variation in interception observed among 12 different plots (Dietz et al., 2006). It is unclear whether the studied plots are representative for a larger forest area. As remote sensing should be capable of identifying forest structure at larger scales, we applied such a technique to a region that includes the stands analyzed in Central Sulawesi (Dietz et al., 2006).

Remote sensing sensors capture forest structure via the varying reflectance intensities of different parts of the tree crown and canopy gaps (de Wasseige and Defourny, 2002). With sensor resolutions higher than the observed crown sizes common approaches to describe canopy related characteristics are based on classification techniques employing first order characteristics like mean and standard deviation of the reflectance intensities. Additional information can be derived from the spatial arrangement of the reflectance intensities. Such second order characteristics like texture measures introduced by Haralick et al. (1973) or the geostatistics based variogram analysis are frequently incorporated in classification processes (Franklin et al., 2000; Jakomulska and Clarke, 2001; Zhang et al., 2004; Lloyd et al., 2004; Puissant et al., 2005).

Although less common first and second order characteristics have been successfully employed in the prediction of forest structure parameters at the stand or plot level. Thenkabail et al. (2004) and Kuplich et al. (2005) both predicted biomass. Thenkabail et al. (2004) utilized first order characteristics of IKONOS data derived normalized difference vegetation indices (NDVI), whereas Kuplich et al. (2005) used texture and variogram analysis derived from synthetic aperture radar (SAR) imagery. Gillespie et al. (2006) predicted stand density based on regression models with NDVI and middle infrared index (MIRI) as regressors. In a similar regression approach both Wulder et al. (1998) and Moskal and Franklin (2004) modeled the relationship between image texture, NDVI, and leaf area index (LAI) where the latter also tried to predict defoliation. St-Onge and Cavaya (1997) as well as Levesque and King (1999, 2003) used variogram based parameters as input to regression models predicting crown diameter, stand density, and crown closure. A set of first and second order characteristics were employed by Muinonen et al. (2001) in the canonical correlation based most similar neighbor approach to predict stand volume at the plot level. The suitability of the different characteristics depends on the spatial resolution of both the sensors and the objects to be modeled.

Summarizing these studies, it can be concluded, that, in general, relationships between the intensity of reflected solar or microwave energy and the horizontal structure of forest stands exist at the stand or plot level and can be modeled using spatio-temporal signatures from remote sensing data. As the studies by Asdak et al. (1998), Chappell et al. (2001), and Dietz et al. (2006) indicate that management-induced changes in rainfall interception are influenced by canopy characteristics the aim of the study was to test different kinds of satellite image characteristics for their suitability to model rainfall interception at the plot level. High correlations between image characteristics and rainfall interception would further the understanding of the influence of canopy structure on the latter. In addition, such correlations would make a regionalization of rainfall interception by the use of satellite images a promising exercise.

The present study was conducted using high-resolution satellite images (Quickbird-2) from the montane rain forest region of Central Sulawesi, Indonesia, where forest structure analyses and rainfall interception studies were conducted (Dietz et al., 2006). The studied forest stands were differently managed by members of the local community (Helmi, 2005) and the land use in the 12 studied stands ranged from natural rain forest with only little rattan extraction to cacao agroforest with some trees left from the original forest.

Investigated characteristics indicating canopy structure were mean and standard deviation of reflectance values. In addition, the spatial arrangement of the reflectance values were described by a set of second order texture measures and variogram based parameters. Furthermore, local maxima of reflectance values were taken into account.

## Methods

### *Field data*

Field data are summarized here in order to give necessary background information for our following analyses. For a detailed discussion see Dietz et al. (2006).

The 12 study plots of 1500 $m^2$ were located at lower montane elevations (800–1140 m asl) in the margin zone of the Lore Lindu National Park in Central Sulawesi, Indonesia (cf. Fig. 1). Four forest use types were selected, (a) natural forest, (b) forest with extraction of small-diameter timbers (hereafter termed 'small timber extraction'), (c) forest with selective extraction of large timbers (hereafter termed 'large timber extraction'), and (d) cacao (*Theobroma cacao*) plantations under trees remaining from the natural forest (agroforest). Slopes ranged between 17° and 39° and all expositions were represented. The annual precipitation close to our plots ranged from 2437 to 3424 mm.

The median basal area of trees $\geqslant$10 cm dbh decreased from 48.1 $m^2\ ha^{-1}$ in the natural forest to 23.4 $m^2\ ha^{-1}$ in the agroforest (Table 1). This was nearly paralleled by a reduction in tree height. The mean height of trees $\geqslant$10 cm dbh decreased from 21.9 to 16.8 m, and the top height (height of the 10 % thickest trees $\geqslant$10 cm dbh) dropped from 42.9 to 33.2 m. The estimated leaf area index, LAI, averaged 6.2 $m^2\ m^{-2}$ in the natural forest, 5.3 in forests with small timber extraction, 5.0 in forests with large timber extraction and 5.4 in the agroforest.

The measurement campaigns for rainfall interception lasted for 15–17 rain days on each plot with daily recording of 30 throughfall gauges and 10 stemflow collectors per plot. The median of throughfall was lowest in natural forest (69.8% of Pg), and similarly high in all other use types (79.1–81.2%). Stemflow was estimated with less than 1% of Pg in all studied use types. Thus, interception was highest in the natural forest where as the median 29.9% of Pg were re-evaporated back into the atmosphere, and much less in the three other use types (17.9–20.0% of Pg). LAI alone did not correlate significantly with the pattern of rainfall partitioning. In a multiple linear regression with tree height and LAI as influencing factors, 81% of the variation in interception percentage is explained.

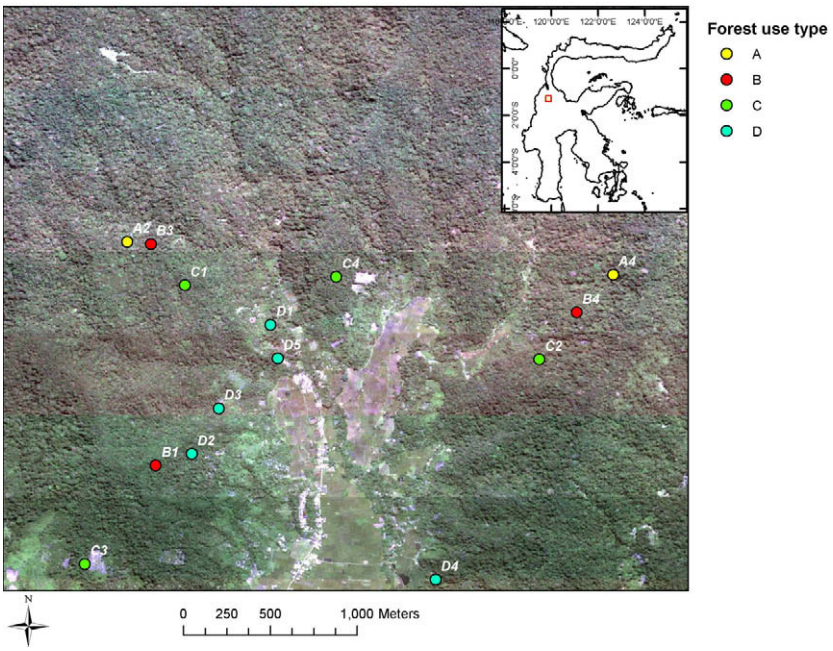


**Figure 1.** Quickbird-2 map of the village of Toro, Central Sulawesi, with superimposed study sites.

**Table 1**
Grey level co-occurrence texture statistics.

| | |
|---|---|
| Contrast | $\sum_{i,j} P_{ij}(i-j)^2$ |
| Entropy | $\sum_{i,j} - P_{ij}\log(P_{ij})$ |
| Correlation | $\sum_{i,j} P_{ij}\frac{(i-\mu_x)(j-\mu_y)}{\sigma_x\sigma_y}$ |

$P_{ij}$ is the co-occurrence probability between grey levels $i$ and $j$ within a local region such that $\sum_{i,j} P_{ij} = 1$, $\mu_x = \sum_{i,j} P_{ij} \times i$, $\sigma_x = \sqrt{\sum_{i,j} P_{ij}(i-\mu_x)^2)}$ and $\mu_x$ and $\sigma_y$ are derived accordingly.

### *Satellite image processing*

The Quickbird-2 satellite data were recorded on April 15, 2004. Quickbird-2 is an optical satellite based sensor operating four spectral bands (blue, green, red, near infrared) at a spatial resolution of 2.88 m and simultaneously one panchromatic band with a spatial resolution of 0.72 m. Both, the multispectral and panchromatic image channels were geometrically and radiometrically corrected prior to statistical analysis. The geometric correction was based on D-GPS measured ground control points (GCP's) and a digital elevation model (DEM) that was generated from topographic maps (1:50.000). The orthorectification algorithm used a rigorous sensor model that accounts for sensor geometry, satellite orbit and topography. The resulting root mean square error (*RMSE*) of the geometric transformation is <1 m.

The radiometric processing included the computation of relative reflectance values, atmospheric correction using the COST-model (Chavez, 1996) and topographic normalization using the stratified Minnaert method (Twele and Erasmi, 2005). The reflectance values were scaled to eight-bit digital numbers using a scaling factor of 1/400.

### *Statistical analyses*

#### *Texture*

As standard first order texture parameters the mean and standard deviation of the grey level values were computed for each object, i.e., the field plots. These parameters were derived separately for the panchromatic band and NDVI data computed from near infrared and red spectral bands.

Additionally, a set of contrast, entropy, and correlation texture parameters was computed for the panchromatic data based on the grey level co-occurrence matrix (GLCM) after Haralick et al. (1973). The grey level co-occurrence matrix can be thought of as a two-dimensional histogram of grey levels of a pair of pixels. The GLCM was computed taking into account all possible directions of co-occurrence (0°, 45°, 90°, 135°). GLCM statistics were extracted at two different levels, the object level and the pixel-level using different window sizes. At the object level, only one co-occurrence matrix was computed covering all pixels representing the field plots on the ground and no grey level quantification was applied. In the pixel based approach, a co-occurrence matrix was computed for every pixel using squared window sizes of 5, 10, 15, and 20 pixel width and the grey level quantification was set to 32 (cf. Clausi, 2002). The texture measure per object was then derived by the mean of all pixels representing the respective field plot.

High local tonal variation will yield a high contrast. Entropy has a high value when the elements of GLCM have relatively equal values and a low value when the local region is rather uniform. Correlation measures the linear dependency of grey levels of neighboring pixels. A summary of the computed texture parameters is given in Table 1.

#### *Variography*

Spatial structure was analysed on the field plot level by means of empirical semi-variograms. The semi-variogram is a measure of spatial correlation and was modeled here as $\gamma(h,\theta)$, with $h$ being a distance vector and $\theta \in \Theta = IR^3_+$ being a vector of the spatial-dependence parameters nugget, sill and range. The range is the distance at which a semi-variogram reaches a constant value, the sill. The semi-variogram model considered was a nugget nested within the spherical model. Let $S$ be the sill and $a$ be the range. The nugget model is of the form

$$\gamma(h) = \begin{cases} 0 & h = 0 \\ S & h > 0 \end{cases} \quad (1)$$

The spherical model is expressed by

$$\gamma(h) = \begin{cases} S(1.5h/a - 0.5(h/a)^3), & 0 \leqslant h \leqslant a \\ S, & a \leqslant h \end{cases} \quad (2)$$

Empirical semi-variogram models were estimated and fitted within the software geoR (Ribeiro and Diggle, 2001) using the robust estimator $\hat{\gamma}_R$ proposed by Cressie and Hawkins (1980). Variogram fitting was based on the Nelder–Maed optimization algorithm using equal weights per bin with lag distance 1 pixel.

*Local maxima*

Local extrema have been frequently employed in forest related digital image processing. The underlying idea is that maximum values are representing tree tops whereas minima or valleys represent gaps or breaks between tree crowns. A valley following approach (Gougeon, 1995; Leckie et al., 2005) is suitable where the spatial resolution is well below the average crown diameter. The technique aims at delineating entire crowns. As the spatial resolution decreases with respect to crown size radiance peak filtering becomes favorable, seeking to identify individual trees by tree top location. The choice of the window size for peak filtering is important (Wulder et al., 2000, 2004) and is quite often accompanied by prior image smoothing with a Gaussian kernel and subsequent thresholding (Dralle and Rudemo, 1996; Uuttera et al., 1998; Pitkänen, 2001; Haara and Nevalainen, 2002; Haara and Haarala, 2002).

The rationale for thresholding is that peaks below a threshold are attributed to variation in the intensity of light at lower branches of trees or structures between trees rather than to the tree tops (Dralle and Rudemo, 1996). As we aimed to capture the crown structure rather than individual trees no thresholding was applied in the current study. A maximum was defined as a pixel or a group of pixels of the panchromatic data with same grey level value having only neighbors whose grey level values were smaller.

In order to reduce noise and increase interpretability the grey level values were additionally smoothed with Gaussian kernels. Kernel sizes of 3, 5, 7 and 11 pixel width were taken into account. The employed filter weights $W_{ij}$ were the normalized values of $G_{ij}$ obtained by the Gaussian function

$$G_{ij} = \exp\left(\frac{-(i-u)^2 - (j-v)^2}{2\sigma^2}\right) \quad (3)$$

where $u$ and $v$ are the center of the kernel and $\sigma^2$ depends on the kernel size $k$, $\sigma^2 = k/2 - 1$, and determines the degree of smoothing (cf. Pitkänen, 2001). The filtered grey level value was derived as

$$BV_{uv} = \sum_{ij} W_{ij} BV_{ij} \quad (4)$$

Local maxima were evaluated at individual grey level value levels.

*Model diagnostics*

Linear product-moment correlation analysis was used to compare variables and to guide variable selection for regression models. Unless mentioned otherwise all significance tests were two sided at the $\alpha = 0.05$ level. Model fit was evaluated in terms of the adjusted coefficient of determination $R^2_{adj}$, the cross-validated root mean square error (*RMSE*), and the ratio *RMSE%* of *RMSE* to the mean interception $\mu_I$

$$RMSE = \sqrt{\sum_{i=1}^{n} (\hat{I}_i - I_i)^2 / n} \quad (5)$$

where $\hat{I}_i$ is the predicted and $I_i$ the measured interception of the plot $i = 1,\ldots,n$ and

$$RMSE\% = RMSE/\mu_I * 100 \quad (6)$$

where $\mu_I = 1/n\sum_{n=1}^{n} I_i$. Cross-validation was done by the leave-one-out procedure; for each plot $i$ a model was fit employing $1,\ldots,i-1,i+1,\ldots,n$ plots. $\hat{I}_i$ was then predicted by applying the model parameters to the $i$th observation. Statistical analysis was conducted with the software R (R, 2006).

## Results

*Linear correlation analysis*

*Texture*

The mean values of the panchromatic and NDVI channels show similar correlations to interception (cf. Table 2). Both correlations of −0.54 and −0.53 are larger in absolute terms than the ones for standard deviation with 0.11 and 0.51. However, due to the low number of 12 observations none of them are significant. With regard to the second order characteristics, only contrast reaches a higher linear relationship with interception than the first order mean grey level values. This implies that apart from contrast measures based on window sizes larger than 5 pixels none of the other second order characteristics correlations with interception are significant. Derivation of contrast, entropy, and correlation at the object level yielded always smaller correlations than the pixel based approaches. For the latter, an increase in window size resulted in higher absolute correlations for contrast and entropy, where the largest correlations were obtained for width of 15 and 20 pixels. An inverse tendency holds for the correlation measure. The product-moment correlation decreases continuously with larger window size.

$\text{Interception}_{10}$ refers to events where precipitation was less equal 10 mm $d^{-1}$. Correlations between the mean and standard deviation of panchromatic data are significant for NDVI data only. As for contrast, entropy, and correlation again the object based approach is inferior to the pixel based one. With $\text{interception}_{10}$ all three texture measures yield higher correlations than with interception. There is a similar trend of increasing absolute correlation

**Table 2**
Pearson's product-moment correlation between satellite image grey level value characteristics and interception (int) and interception when precipitation was less than 10 mm $d^{-1}$($\text{int}_{10}$).

| | int | $\text{int}_{10}$ | | int | $\text{int}_{10}$ |
|---|---|---|---|---|---|
| $\text{mean}_{\text{Pan}}$[c] | −0.54 | −0.56 | $\text{nugget}_{\text{Pan}}$[c] | 0.12 | 0.31 |
| $\text{sd}_{\text{Pan}}$ | 0.11 | −0.54 | $\text{sill}_{\text{Pan}}$[c] | 0.30 | 0.56 |
| $\text{mean}_{\text{NDVI}}$[d] | −0.53 | −0.64 | $\text{range}_{\text{Pan}}$ | 0.28 | 0.42 |
| $\text{sd}_{\text{NDVI}}$ | 0.51 | 0.76 | $\text{nugget}_{\text{NDVI}}$ | 0.21 | −0.17 |
| $\text{Contrast}_{\text{Obj}}$[a] | −0.37 | −0.58 | $\text{sill}_{\text{NDVI}}$ | 0.42 | 0.79 |
| $\text{Contrast}_{5\times5}$[b] | −0.57 | −0.72 | $\text{range}_{\text{NDVI}}$ | 0.15 | 0.54 |
| $\text{Contrast}_{10\times10}$ | −0.60 | −0.74 | LM | 0.80 | 0.64 |
| $\text{Contrast}_{15\times15}$ | −0.61 | −0.75 | $\text{LM1}_{3\times3}$[b,e] | 0.66 | −0.63 |
| $\text{Contrast}_{20\times20}$ | −0.61 | −0.75 | $\text{LM1}_{5\times5}$ | 0.73 | −0.74 |
| $\text{Entropy}_{\text{Obj}}$ | −0.19 | −0.04 | $\text{LM1}_{7\times7}$ | 0.57 | −0.48 |
| $\text{Entropy}_{5\times5}$ | −0.32 | −0.66 | $\text{LM1}_{9\times9}$ | 0.73 | 0.61 |
| $\text{Entropy}_{10\times10}$ | −0.41 | −0.61 | $\text{LM1}_{11\times11}$ | 0.83 | 0.70 |
| $\text{Entropy}_{15\times15}$ | −0.42 | −0.61 | $\text{LM2}_{3\times3}$[b,e] | 0.72 | 0.61 |
| $\text{Entropy}_{20\times20}$ | −0.42 | −0.56 | $\text{LM2}_{5\times5}$ | 0.74 | 0.54 |
| $\text{Correlation}_{\text{Obj}}$ | 0.12 | 0.64 | $\text{LM2}_{7\times7}$ | 0.78 | 0.81 |
| $\text{Correlation}_{5\times5}$ | 0.50 | 0.57 | $\text{LM2}_{9\times9}$ | 0.74 | 0.55 |
| $\text{Correlation}_{10\times10}$ | 0.41 | 0.73 | $\text{LM2}_{11\times11}$ | −0.38 | −0.56 |
| $\text{Correlation}_{15\times15}$ | 0.31 | 0.68 | | | |
| $\text{Correlation}_{20\times20}$ | 0.18 | 0.61 | | | |

[a] Texture derivation at the object level.
[b] Numbers refer to the employed window size.
[c] Panchromatic channel data.
[d] NDVI channel data.
[e] LM1 local maxima with one-time smoothing, LM2 local maxima with two-times smoothing; sd = standard deviation.

with increasing window size for contrast. The largest absolute correlations of −0.75 are obtained again for widths of 15 and 20 pixels. For entropy this time there is a decreasing tendency of the achieved absolute correlation with increasing window sizes. For the correlation measure the product-moment correlation increases from window size 5–10 to 0.73 and decreases again for larger window sizes down to 0.61.

*Variography*

Although the semi-variograms of the grey level values showed clearly discernable different shapes for both panchromatic and NDVI data none of the derived parameters had a significant linear relationship with interception. Except from the sill of NDVI data the semi-variogram approach was inferior to all other approaches in terms of linear correlation.

As with the texture measures the semi-variogram parameters also yielded higher correlations with $\text{interception}_{10}$. However, only the correlation of 0.79 of sill of NDVI data is significant and resulted into the second to highest overall correlation.

*Local maxima*

The local maximum technique yielded quite promising results. The values listed in Table 2 are based on the maxima of the grey level value having the highest product-moment correlation with interception. Without smoothing the second to highest correlation of 0.80 was achieved. However, maxima of the underlying grey level values were observed only on two plots. The high correlation can be explained by the leverage the maxima of the two plots exert.

With one-time Gaussian smoothing no clear relationship between kernel size and correlation is discernable with kernel widths of 5 and 9 pixels yielding the same correlation of 0.73, outperforming the kernels of width of 3 and 7 pixels. The highest overall correlation of 0.83 was obtained with the largest kernel of width 11 pixels. Local maxima were observed on 5 out of the 12 plots for a brightness value of 53. With two-times smoothing there is an increase of correlation with increasing kernel width until a size of 7 pixels. The correlations decrease with larger kernel sizes and even switch signs for the approach based on the largest kernel.

Local maxima of the un-smoothed data yielded a correlation with $\text{interception}_{10}$ within the range of the texture and variography approaches. Varying kernel sizes resulted in no clear trends for both smoothing approaches. For one-time smoothing the correlation decreases first and then increases, switches sign between kernel size seven and nine and peaks for the largest kernel size. However, this correlation of 0.70 is smaller in absolute terms than the one for kernel size five with −0.74. For two-time smoothing correlations undulate with a peak of 0.81 for a kernel size of seven and a subsequent decrease with switch of signs between kernel sizes 9 and 11.

*Regression analysis*

The robustness of the linear relationship between interception and satellite image grey level value characteristics were tested with cross-validated regression analysis. Using just $\text{LM1}_{11\times11}$ as regressor yielded a significant adjusted coefficient of determination of 0.65. The relative *RMSE* of 44.2% is quite high (cf. Table 3). In order to consider as many grey level value characteristics as possible a stepwise regression approach was followed (Venables and Ripley, 2002). Input variables were $\text{LM1}_{11\times11}$, $\text{Entropy}_{15\times15}$, $\text{Correlation}_{5\times5}$, $\text{Contrast}_{15\times15}$, $\text{mean}_{\text{Pan}}$, $\text{mean}_{\text{NDVI}}$, $\text{range}_{\text{Pan}}$, $\text{range}_{\text{NDVI}}$, $\text{sill}_{\text{Pan}}$, $\text{sill}_{\text{NDVI}}$, $\text{sd}_{\text{Pan}}$, and $\text{sd}_{\text{NDVI}}$. The stepwise regression algorithm selects variables on basis of Akaike's information criterion AIC. If the algorithm proposed non-significant regressors, the one with the lowest absolute *t*-value was excluded and the stepwise regression re-run with the remaining variables. With this approach a model with $\text{LM1}_{11\times11}$, $\text{Contrast}_{15\times15}$, and $\text{mean}_{\text{NDVI}}$ as regressors was selected. All three input variables were significant and a Shapiro test on the distribution of the residuals showed no significance. Except for an agroforest stand with very low interception plotting the measured versus predicted interception showed good agreement (Fig. 2). The obtained adjusted coefficient of determination of 0.84 outperformed the best regression model based on in the field measured variables mean tree height and LAI (cf. Dietz et al., 2006). The improvement of the relative *RMSE* from 37.6% down to 26.7% was even more pronounced.

**Table 3**
Regression statistics of final models, interception as dependent variable.

| Predictors | $R^2_{adj}$ | *p*-value | *RMSE* | *RMSE*% |
|---|---|---|---|---|
| $\text{LM1}_{11\times11}$[a,b] | 0.65 | <0.001 | 9.5 | 44.2 |
| $\text{LM1}_{11\times11}$ + $\text{Contrast}_{15\times15}$ + $\text{mean}_{\text{NDVI}}$[c] | 0.84 | <0.001 | 5.73 | 26.7 |
| mHeight[d] | 0.60 | 0.002 | 10.62 | 49.4 |
| mHeight + LAI | 0.79 | <0.001 | 8.08 | 37.6 |

[a] LM1 local maxima with one-time smoothing.
[b] Numbers refer to the employed window size.
[c] NDVI channel data.
[d] Mean tree height as measured on the ground.

With 12 observations and three explanatory variables in the final regression model a selection based on the coefficient of determination can be misleading as this measure does not capture model over fit. The employed adjusted coefficient of determination serves to compare fit among models but is also prone to model over-specification. Robustness was checked by the variance inflation factor of the regressors which with a maximum of 3.3 is below the threshold of five stated by Montgomery et al. (2006). The robustness of the final model was corroborated by the small *RMSE*.

In order to apply the regression model on a landscape level an area surrounding Toro village roughly representing a bound box of the 12 research plots was divided into grid cells of 1500 $m^2$ each. Known residential areas were masked out leaving a total of 5224 cells covering 783.6 ha (cf. Fig. 3). For each cell the mean NDVI value, contrast of panchromatic data using a $15\times15$ window, and local maxima of brightness value 53 after one-time

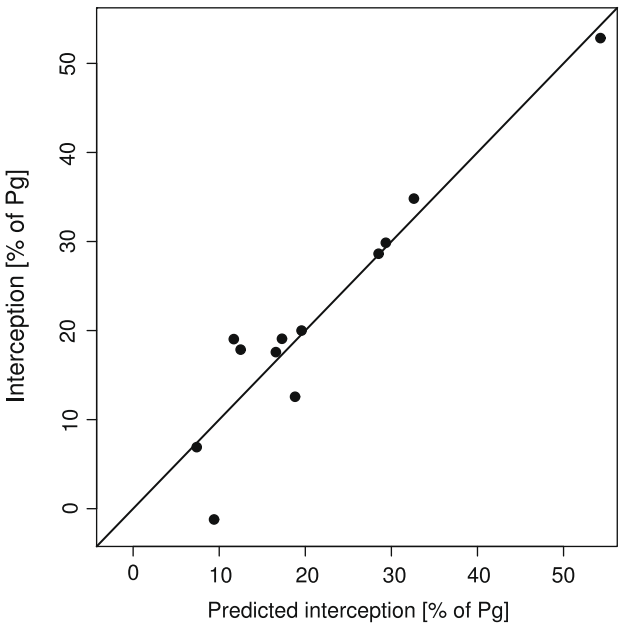


**Figure 2.** Measured versus predicted interception.

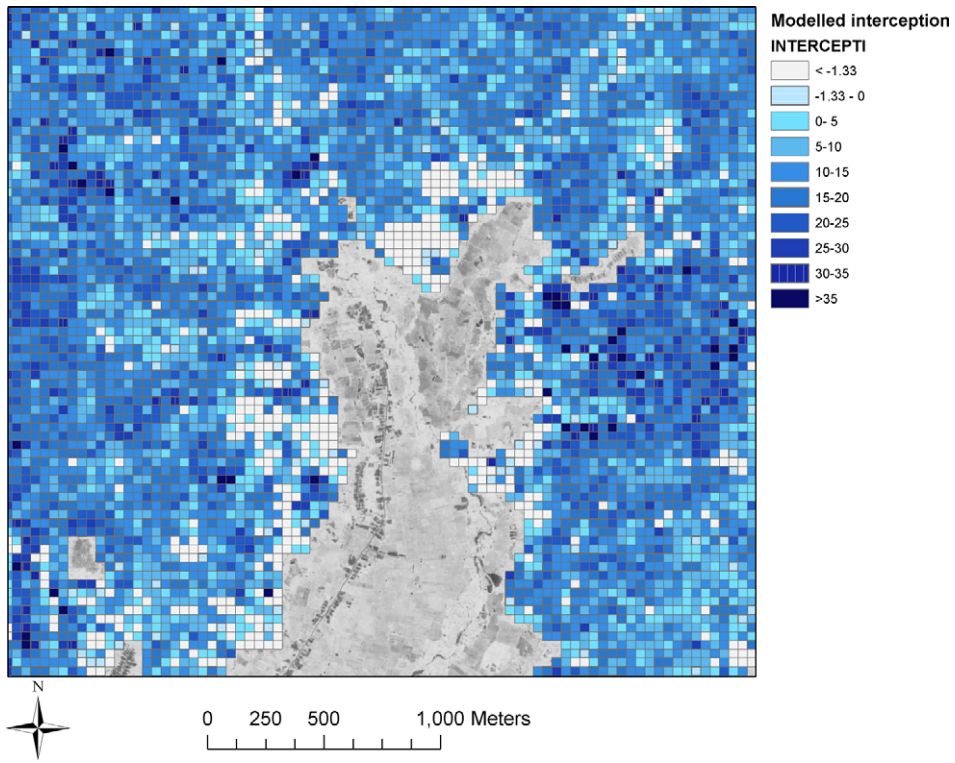


**Figure 3.** Modeled interception for 783.6 ha of forests surrounding Toro valley. Paddy rice and residential areas were masked out.

smoothing with an 11 × 11 window were derived. The histogram of the predicted interception values (Fig. 4) display a realistic scenario where values over 30% are scarce. The spatial distribution of predicted interception (Fig. 3) reflects well the anticipated patterns with rare peaks just below ridges and lowest interception towards the lower hill slopes (cf. Fig. 1). The latter are traditionally subject to highly intensive forest management as cacao agroforests.

## Discussion

Rainfall interception from natural forest in the montane region of Central Sulawesi was 30% of Pg on the median and is thus higher than in the above cited lowland sites on Borneo (Asdak et al., 1998; Chappell et al., 2001). In Southeast Asian lowland forests, high interception rates were reported for stands in Brunei and Sarawak close to the South China Sea (Dykes, 1997; Kumagai et al., 2005).

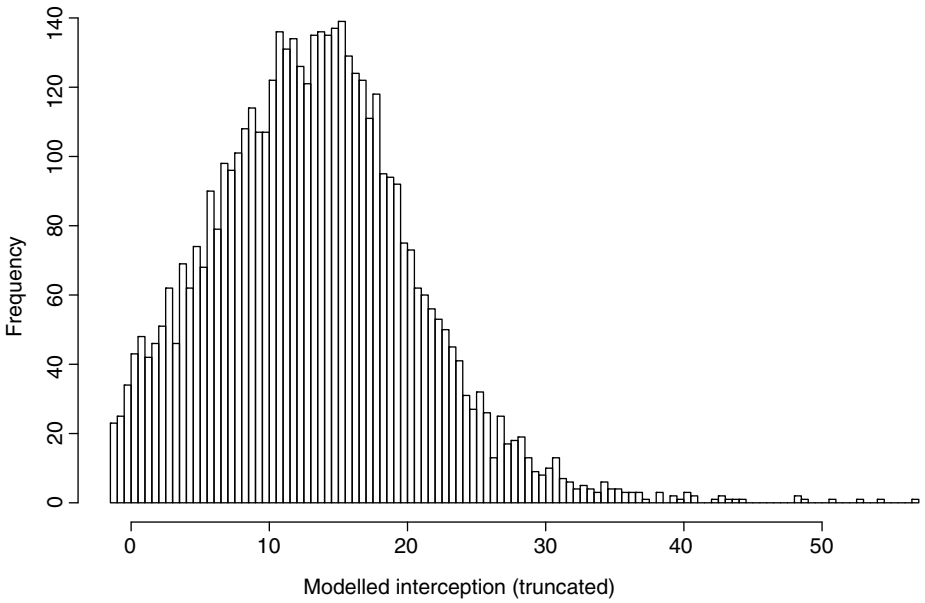


**Figure 4.** Histogram of modeled interception per 1500 $m^2$ grid cell. The histogram is truncated below −1.5% and above 58%.

The median rainfall interception in Sulawesi is within the range observed for other montane forests not subject to substantial cloud incidence. The extensive literature reviews by Bruijnzeel and Proctor (1995) and Bruijnzeel (2001) give values between 20% and 37% of Pg. However, our investigated stands in the montane rain forest show some local specific features. In one of the natural forest stands we observed a rainfall interception of 53% and in one of the agroforest stands we resulted at −1%. From a statistical viewpoint the latter result proved to be an outlier in the regression analysis. We regarded our measurement scheme for throughfall and stemflow as quite robust and could not distinguish sources of error for specific stands. We thus opted to maintain the full observed data variability of results in the further analyses.

There are few comparable studies known to the authors. The paucity of studies is due to the difficult to collect field data, and the required integration of detailed ecological knowledge from field research (Chambers et al., 2007). Gillespie et al. (2006) used Landsat 7 ETM+ derived spectral indices like NDVI for modeling of structure of tropical dry forests. Structure parameters investigated included density, basal area, and maximum tree height, assessed at the stand level. Groeneveld and Baugh (2007) also used Landsat TM based NDVI data investigating hydrological response of vegetation but the study sites were located outside the tropics. The resolution of Landsat imagery with 30 m is too coarse with respect to plot sizes used in interception studies, representing usually less than 3 pixels (Dietz et al., 2006; Vernimmen et al., 2007).

The potential of IKONOS data in ecological applications in Amazonia has been evaluated by related studies (Read et al., 2003; Hurtt et al., 2003; Clark et al., 2004). The employed IKONOS data are similar to the Quickbird data utilized in this work. A first approach was confined to visual interpretation and manual digitization of tree crowns and found a significant albeit weak correlation (Read et al., 2003). In a next step first results of automated crown detection techniques were introduced (Hurtt et al., 2003). A study on automated derivation of IKONOS imagery characteristics yielded useful data on tree size and location, mortality and growth (Clark et al., 2004) where the structural variable percentage of plot area with canopy above 15 m was most frequently correlated with some aspect of the IKONOS panchromatic data. The field data consist of 18 0.5 ha plots and thus reflects the challenge of establishing a sufficient data basis.

Vernimmen et al. (2007) provide an overview of the parameters of the most widely used interception models characterizing the canopy. Of the four investigated parameters, canopy saturation, free throughfall, and the proportion of rain diverted to the trunks can be modeled based on remotely sensed imagery. The spatial patterns of trees have a considerable effect on the magnitude and distribution of canopy reflectance (de Wasseige and Defourny, 2002), leaving only trunk water storage capacity uncovered.

Canopy saturation relates to LAI and free throughfall is inverse proportional to gap fraction. The latter can be considered a surrogate for canopy roughness but does not account for gap distribution, size, density, or depth used in the modeling approach by de Wasseige and Defourny (2002). Vernimmen et al. (2007) had difficulties predicting the measured interception by the chosen models. They concluded that they severely overestimated the interception at one site as inverse modeling yielded unrealistic parameters. However, their chosen model does not account for size and frequency of rain fall which Hall (2003) found to be one of the main contributing factors. An influence of rain fall intensity on interception would help explain our findings that our derived image characteristics correlated stronger with interception when precipitation was less than 10 mm $d^{-1}$.

The conclusion reached by Hall (2003) that further studies should concentrate on the representation of the canopy like distribution of canopy elements is partly realized in the splash droplet approach of Murakami (2006). The spatial canopy structure will also affect interception as the tree architecture, angle and surface state of leaves would influence the distribution of the splash droplet size distribution, which he found contributes to interception and can help overcome contradictions of established interception models.

In our study, the modeling of interception is compounded by the small number of observations, which, nevertheless, cover a wide range of interception values. The one extreme value of 53% exerted high leverage in the correlation and regression analysis, rendering measures that capture or keep high detail superior over measures that tend to smooth the underlying data. For example, for second order statistics, all object derived statistics were inferior to their pixel based counterparts which is attributed to the grey level quantification of the latter. Performance was less influenced by the chosen window size and leveled off for contrast between 10 and 15 pixel width, corresponding to 7–11 m on the ground. These dimensions seem representative with smaller windows not capturing the underlying structure. Contrast measures the average tonal variation within the field plot and indicates here that the lower the variation of the reflectance intensities within the canopy the higher the observed interception.

Local maxima are the only measure derived directly from the underlying reflectance values. All other introduced measures rely on averaging or some kind of smoothing transformation during their derivation. For the given data local maxima had the highest modeling power due to their capability to capture the field plots with high interception and leverage quite well. Pooling several brightness values or even thresholding diminished the modeling power of local maxima. Also employing relative maxima derived as the difference to their mean value per-field plot did not prove to be efficient.

Our plots showed different variograms with ranges mainly between 7 and 17 pixels for both panchromatic and NDVI data. However, we were surprised to find that variography analysis was of little use with respect to modeling interception. Semivariogram parameters yielded high coefficients of determination in models of canopy closure and tree crown size (Levesque and King, 1999; St-Onge and Cavaya, 1997) and we assumed these surrogates of canopy structure to have an association with interception.

A possible explanation is that when applied to several land cover types modeling power of the range may be diminished as semi-variograms are shift invariant and gaps as well as crowns can produce similar values. Interpretation of a range needs to consider the sill as well. However, even jointly regarded these two measures did not prove significant in the regression analysis.

For the current modeling approach the spatial resolution of 2.88 m of the multispectral Quickbird image proved to be too coarse except for the simple measures mean, variance, or sill, which is closely related to variance. The higher spectral resolution on which the NDVI data relies compensated for the loss in spatial resolution as the mean value of NDVI was significant in the multiple regression and improved model fit.

For the selected area the applied modeling methodology yielded reasonable and robust results. In general, a transfer of models to other study areas is difficult (Lu, 2006). Extending the model to other regions or even increasing the predicted area around Toro village beyond the bounding box of the existing research plots would require additional study sites. The regionalized area should be well covered by the study sites with respect to topography and forest use intensity.

## Conclusion

An increase in forest use intensity changed the forest structure and significantly reduced rainfall interception in the montane zone

of Central Sulawesi, Indonesia. The change in forest structure affects the distribution of the canopy reflectance of solar radiation. High-resolution optical space borne imagery proved to be suitable to capture the variability and changes in forest structure and by means of derived texture characteristics can successfully be applied to the regional prediction of interception.

Understanding the association between textural measures of high-resolution remote sensing data and canopy structure is not straightforward (cf. Kuplich et al., 2005). In our study the prediction power of textural measures at the object level was always lower compared to local neighborhood derived ones. In general, linear correlations between interception when precipitation was less than 10 mm $d^{-1}$ and brightness value characteristics were higher than for overall interception indicating that the chosen regressors do not capture all contributing factors. Still, the derived linear regression model was able to explain more than 84% ($R^2_{adj}$) of the variation encountered in the data, was stable with respect to cross-validation, and yielded realistic distributions with respect to values and their spatial alignment when applied to a 783.6 ha subset of the study area.

Local maxima of the reflectance values were the single most contributing factor in our final model. The additional analysis of their spatial alignment as a point pattern (Nelson et al., 2002) would allow for the description of the forest canopy structure at a level of detail we found to be important in modeling interception. This technique is not restricted to optical sensors but can also be applied to LIDAR data and would further increase the potential of this data source (Roth et al., 2007). Such approaches should yield better approximations of characteristics related to interception and with the integration of detailed ecological knowledge can contribute to the understanding of interception and guide future field work.

## Acknowledgements

This study was conducted in the framework of the joint Indonesian-German research project "Stability of Tropical Rainforest Margins, Indonesia (STORMA)" funded by the German Science Foundation (SFB 552).

We applied the "first-last-author-emphasis" norm (FLAE) as suggested by Tscharnkte et al. (2007).

## References

Achard, F., Eva, H.D., Stibig, H.J., Mayaoux, P., Gallego, J., Richards, T., Malingreau, J.P., 2002. Determination of deforestation rates of the world's humid tropical forests. Science 297, 999–1002.

Asdak, C., Jarvis, P.G., van Gardingen, P., Fraser, A., 1998. Rainfall interception loss in unlogged and logged forest areas of Central Kalimantan, Indonesia. J. Hydrol. 206, 237–244.

Asner, G.P., Knapp, D.E., Broadbent, E.N., Oliveira, P.J.C., Keller, M., Silva, J.N., 2005. Selective logging in the Brazilian Amazon. Science 310, 480–482.

Bruijnzeel, L.A., 1990. Hydrology of Tropical Forests and Effects of Conversion: A State of Knowledge Review. UNESCO/Vrije Universiteit, Paris/Amsterdam. 224p.

Bruijnzeel, L.A., 2001. Hydrology of tropical montane cloud forests: a reassessment. Land Use Water Res. 1, 1.1–1.18.

Bruijnzeel, L.A., Proctor, J., 1995. Hydrology and biochemistry of tropical montane cloud forests: what do we really know? In: Hamilton, L.S., Juvik, J.O., Scatena, F.N. (Eds.), Tropical montane cloud forests, Ecological Studies, vol. 110. Springer, Berlin, pp. 38–78.

Chambers, J.Q., Asner, G.P., Morton, D.C., Anderson, L.O., Saatchi, S.S., Espirito-Santo, F.D.B., Palace, M., Souza, C., 2007. Regional ecosystem structure and function: ecological insights from remote sensing of tropical forests. Trends Ecol. Evol. doi:10.1016/j.tree.2007.05.001.

Chappell, N.A., Bidin, K., Tych, W., 2001. Modelling rainfall and canopy controls on net-precipitation beneath selectively-logged tropical forest. Plant Ecol. 153, 215–229.

Chappell, N.A., Tych, W., Yusop, Z., Rahim, N.A., Kasran, B., 2005. Spatially significant effects of selective tropical forestry on water, nutrient and sediment flows: a modelling-supported review. In: Bonnell, M., Bruijnzeel, L.A. (Eds.), Forests, Water and People in the Humid Tropics. Cambridge University Press, Cambridge, pp. 513–532.

Chavez Jr., P.S., 1996. Image-based atmospheric corrections – revisited and improved. Photogramm. Eng. Remote Sens. 62 (9), 1025–1036.

Clark, D.B., Read, J.M., Clark, M.L., Cruz, A.M., Dotti, M.F., Clark, D.A., 2004. Application of 1-m and 4-m resolution satellite data to ecological studies of tropical rain forests. Ecol. Appl. 14 (1), 61–74.

Clausi, D.A., 2002. An analysis of co-occurrence texture statistics. Can. J. Remote Sens. 28 (1), 45–62.

Cressie, N., Hawkins, D.M., 1980. Robust estimation of the variogram: I. Math. Geology 12 (2), 115–125.

de Wasseige, C., Defourny, P., 2002. Retrieval of tropical forest structure characteristics fro bi-directional reflectance of SPOT images. Remote Sens. Environ. 83, 362–375.

Dietz, J., Hölscher, D., Leuschner, C., Hendrayanto, 2006. Rainfall partitioning in relation to forest structure in differently managed montane forest stands in Central Sulawesi, Indonesia. Forest Ecol. Manage. 237, 170–178.

Dralle, K., Rudemo, M., 1996. Stem number estimation by kernel smoothing of aerial photos. Can. J. Forest Res. 26, 1228–1236.

Dykes, A.P., 1997. Rainfall interception from a lowland tropical rainforest in Brunei. J. Hydrol. 200, 260–279.

Erasmi, S., Twele, A., Ardiansyah, M., Malik, A., Kappas, M., 2004. Mapping deforestation and land cover conversion at the rainforest margin in Central Sulawesi, Indonesia. EARSeL Proc. 3 (3), 388–397.

FAO (Food Agriculture Organisation of the United Nations), 2001. Global Forest Resources Assessment 2000. FAO, Rome.

Fleischbein, K., Wilcke, W., Valarezo, C., Zech, W., Knoblich, K., 2006. Water budgets of three small catchments under montane forest in Ecuador: experimental and modelling approach. Hydrol. Process. 20, 2491–2507.

Franklin, S.E., Hall, R.J., Moskal, L.M., Maudie, A.J., Lavigne, M.B., 2000. Incorporating texture into classification of forest species composition from airborne multispectral images. Int. J. Remote Sens. 21 (1), 61–79.

Gillespie, T.W., Zutta, B.R., Early, M.K., Saatchi, S., 2006. Predicting and quantifying the structure of tropical dry forests in South Florida and the Neotropics using spaceborne imagery. Global Ecol. Biogeogr. 15 (3), 225–236.

Gougeon, F.A., 1995. A crown-following approach to the automatic delineation of individual tree crowns in high spatial resolution aerial images. Can. J. Remote Sens. 21, 274–284.

Grip, H., Fritsch, J.-M., Bruijnzeel, L.A., 2005. Soil and water impacts during forest conversion and stabilisation of new land use. In: Bonnell, M., Bruijnzeel, L.A. (Eds.), Forests, Water and People in the Humid Tropics. Cambridge University Press, Cambridge, pp. 561–589.

Groeneveld, D.P., Baugh, W.M., 2007. Correcting satellite data to detect vegetation signal for eco-hydrologic analyses. J. Hydrol. 344, 135–145.

Haara, A., Haarala, M., 2002. Tree species classification using semi-automated delineation of trees on aerial images. Scand. J. Forest Res. 17, 556–565.

Haara, A., Nevalainen, S., 2002. Detection of dead or defoliated spruces using digital aerial data. Forest Ecol. Manage. 160, 97–1007.

Hall, R.L., 2003. Interception loss as a function of rainfall and forest types: stochastic modeling for tropical canopies revised. J. Hydrol. 185, 1–12.

Haralick, R.M., Shanmugan, K., Dinstein, I., 1973. Textural features for image classification. IEEE Trans. Syst. Man Cybernet. 3 (6), 610–621.

Held, A.A., Rodriguez, E., 2005. Remote sensing tools in tropical forest hydrology: new sensors. In: Bonnell, M., Bruijnzeel, L.A. (Eds.), Forests, Water & People in the Humid Tropics. Cambridge University Press, Cambridge, pp. 598–621.

Helmi, I., 2005. Local people are well-placed to develop zonation plans in Indonesia's Lore Lindu National Park. Trop. Forest Update 15, 31–32.

Hurtt, G., Xiao, X., Keller, M., Palace, M., Asner, G.P., Braswell, R., Brondizio, E.S., Cardoso, M., Carvalho, C.J.R., Fearon, M.G., Guild, L., Hagen, S., Hetrick, S., Moore, B., Read, C., Nobre, J.M., Sa, T., Schloss, A., Vourlitis, G., Wickel, A.J., 2003. IKONOS imagery for the large scale biosphere–atmosphere experiment in Amazonia (LBA). Remote Sens. Environ. 88, 111–127.

Jakomulska, A., Clarke, K.C., 2001. Variogram-derived measures of textural image classification. In: Monestiez et al. (Eds.), Geostatistics for Environmental Applications, geoENV, vol. 3. Kluwer Academic Publishers, pp. 345–355.

Kumagai, T., Saitoh, T.M., Sato, Y., Takahashi, H., Manfroi, O.J., Morooka, T., Kuraji, K., Suzuki, M., Yasunari, T., Komatsu, H., 2005. Annual water balance and seasonality of evapotranspiration in a Bornean tropical rainforest. Agric. Forest Meteorol. 128, 81–92.

Kuplich, T.M., Curran, P.J., Atkinson, P.M., 2005. Relating SAR image texture to the biomass of regenerating tropical forests. Int. J. Remote Sens. 26 (21), 4829–4854.

Leckie, D.G., Gougeon, F.A., Tinis, S., Nelson, T., Burnett, C.N., Paradine, D., 2005. Automated tree recognition in old growth conifer stands with high resolution digital imagery. Remote Sens. Environ. 94, 311–326.

Levesque, J., King, D.J., 1999. Airborne digital camera image semivariance for evaluation of forest structural damage at an acid mine site. Remote Sens. Environ. 68, 112–124.

Levesque, J., King, D.J., 2003. Spatial analysis of radiometric fractions from high-resolution multispectral imagery for modelling individual tree crown and forest canopy structure and health. Remote Sens. Environ. 84, 589–602.

Lloyd, C., Berberoglu, S., Curraan, P., Atkinson, P., 2004. A comparison of texture measures for the per-field classification of Mediterranean land cover. Int. J. Remote Sens. 25 (19), 3943–3965.

Lu, D., 2006. The potential and challenge of remote sensing-based biomass estimation. Int. J. Remote Sens. 27 (7), 1297–1328.

Montgomery, D.C., Peck, E.A., Vining, G.G., 2006. Introduction to Linear Regression Analysis, fourth ed. Wiley & Sons.

Moskal, L.M., Franklin, S.E., 2004. Relationship between airborne multispectral image texture and aspen defoliation. Int. J. Remote Sens. 25 (14), 2701–2711.
Muinonen, E., Maltamo, M., Hyppänen, H., Vainikainen, V., 2001. Forest stand characteristics estimation using a most similar neighbor approach and image spatial structure information. Remote Sens. Environ. 78, 223–228.
Murakami, S., 2006. A proposal for a new forest canopy interception mechanism: Splash droplet evaporation. J. Hydrol. 319, 72–82.
Nelson, T., Niemann, K.O., Wulder, M.A., 2002. Spatial statistical techniques for aggregating point objects extracted from high spatial resolution remotely sensed imagery. J. Geograph. Syst. 4, 423–433.
Pitkänen, J., 2001. Individual tree detection in digital aerial images by combining locally adaptive binarization and local maxima methods. Can. J. Forest Res. 31, 832–844.
Puissant, A., Hirsch, J., Weber, C., 2005. The utility of texture analysis to improve per-pixel classification for high to very high spatial resolution imagery. Int. J. Remote Sens. 26 (4), 733–745.
R Development Core Team, 2006. R: A Language and Environment for Statistical Computing. R Foundation for Statistical Computing Vienna, Austria. ISBN 3-900051-07-0.
Read, J.M., Clark, D.B., Venticinque, E.M., Moreira, M.P., 2003. Application of merged 1-m and 4-m resolution satellite data to research and management in tropical forests. J. Appl. Ecol. 40, 592–600.
Ribeiro Jr., P.J., Diggle, P.J., 2001. geoR: a package for geostatistical analysis. R-NEWS 1 (2), 14–18.
Roth, B.E., Slatton, K.C., Cohen, M.J., 2007. On the potential for high-resolution lidar to improve rainfall interception estimates in forest ecosystems. Front Ecol. Environ. 5 (8), 421–428.
St-Onge, B.A., Cavaya, F., 1997. Automated Forest Structure Mapping from High Resolution Imagery Base on Directional Semivariogram Estimates. Remote Sens. Environ. 61, 82–95.
Thenkabail, P., Stucky, N., Griscom, B., Ashton, M., Diels, J., van der Meer, B., Enclona, E., 2004. Biomass estimation and carbon stock calculations in the oil palm plantations of Africa derived savannas using IKONOS data. Int. J. Remote Sens. 25 (23), 5447–5472.
Tscharnkte, T., Hochberg, M.E., Rand, T.A., Resh, V.H., Krauss, J., 2007. Author sequence and credit for contributions in multiauthored publications. PLoS Biol. 5 (1), e18. doi:10.1371/journal.pbio.0050018.
Twele, A., Erasmi, S., 2005. Optimierung der topographischen normalisierung optischer satellitendaten durch einbeziehung von kohärenzinformation. Photogram. Fernerkundung Geoinform (PFG) 3, 227–234.
Uuttera, J., Haara, A., Tokola, T., Maltamo, M., 1998. Determination of the spatial distribution of trees from digital aerial photographs. Forest Ecol. Manage. 110, 275–282.
Venables, W.N., Ripley, B.D., 2002. Modern Applied Statistics with S, fourth ed. Springer, New York.
Vernimmen, R.R.E., Bruijnzeel, L.A., Romdoni, A., Proctor, J., 2007. Rainfall interception in three contrasting lowland forest types in Central Kalimantan, Indonesia. J. Hydrol. 340, 217–232.
Wulder, M.A., LeDre, E.F., Franklin, S.E., Lavigne, M.B., 1998. Aerial image texture information in the estimation of northern deciduous and mixed wood forest leaf area index (LAI). Remote Sens. Environ. 64, 64–76.
Wulder, M., Niemann, K.O., Goodenough, D.G., 2000. Local maximum filtering for the extraction of tree locations and basal area from high spatial resolution imagery. Remote Sens. Environ. 73, 103–114.
Wulder, M.A., White, J., Niemann, K.O., Nelson, T., 2004. Comparison of airborne and satellite high spatial resolution data for the identification of individual trees with local maxima filtering. Int. J. Remote Sens. 25 (11), 2225–2232.
Zhang, C., Franklin, S.E., Wulder, M.A., 2004. Geostatistical and texture analysis of airborne-acquired images used in forest classification. Int. J. Remote Sens. 25 (4), 859–865.